

NMRlipids IV: Headgroup & glycerol backbone structures, and cation binding in bilayers with PS lipids

Pavel Buslaev,¹ Fernando Favela,² Tiago M. Ferreira,³ Ivan Gushchin,¹ Matti Javanainen,⁴ Batuhan Kav,⁵ Jesper J. Madsen,⁶ Markus Miettinen,⁵ Josef Melcr,⁴ Ricky Nencini,⁴ O. H. Samuli Ollila,^{4,7,*} and Thomas Piggot^{1, Authorlist is not yet complete}⁸

¹*Moscow Institute of Physics and Technology*

²*Mexico*

³*NMR group - Institut for Physics, Martin-Luther University Halle-Wittenberg*

⁴*Institute of Organic Chemistry and Biochemistry, Academy of Sciences of the Czech Republic, Prague 6, Czech Republic*

⁵*Department of Theory and Bio-Systems, Max Planck Institute of Colloids and Interfaces, 14424 Potsdam, Germany*

⁶*Department of Chemistry, The University of Chicago, Chicago, Illinois 60637, United States of America*

⁷*Institute of Biotechnology, University of Helsinki*

⁸*Southampton, United Kingdom*

(Dated: March 6, 2019)

Phosphatidylserine (PS) is a negatively charged lipid commonly found in eukaryotic membranes, where it interacts with signaling and other proteins via electrostatic interactions and direct binding, and can induce membrane fusion and phase separation in the presence of calcium ions. Molecular details of these phenomena are not well understood, because accurate models to interpret the experimental data have not been available. Here, we use solid-state NMR S-DROSS experiments to measure the signs of the previous set of experimental NMR order parameter magnitudes available for POPS to assess the phosphoserine structure in the different atomistic force-fields presently used. We also gather a set of experimental NMR data that can be used to assess the ion binding to pure PS and mixed PC:PS lipid bilayers in molecular dynamics (MD) simulations. Using the open collaboration method, we extract data from wide range of available PS MD models (force fields) and perform a comparison to NMR results. We find that none of the models reproduce the NMR data within experimental accuracy, but the best ones suggest that the carboxyl group in the serine headgroup does not rotate freely. In line with the previous results for PC lipids, none of the PS force fields correctly captures the cation binding affinity. Furthermore, the response of PS headgroups to bound ions *qualitatively* differs from experiments. The collected experimental dataset and simulation results pave the way for improvement of lipid force fields to correctly describe the biologically relevant negatively charged membranes and their interactions with ions. This work is part of the NMRlipids open collaboration project (nmrlipids.blogspot.fi).

INTRODUCTION

Phosphatidylserine (PS) is the most common negatively charged lipid in eukaryotic membranes. PS lipids compose 8.5% of total lipid weight of red blood cells. The abundance, however, varies between different organelles, and up to 25-35% of the cytosolic leaflet of plasma membranes [1–3] consists of PS lipids. PS lipids are vastly important signaling molecules. They interact with signaling proteins [2], regulate surface charge and protein localization [4], and induce protein aggregation [5, 6]. Some protein domains interact specifically with PS lipids, while other protein sites are attracted by nonspecific electrostatics and the binding can be regulated by calcium [2]. Therefore, the structural details of lipid headgroups and the details of cation binding are crucial for the PS-mediated signaling processes.

Experimental studies have indicated that the PS headgroup is more rigid than the phosphatidylcholine (PC) due to hydrogen bonding network or electrostatic interactions [7, 8]. While monovalent ions interact weakly with PS-containing bilayers, multivalent cations and Li^+ are able to form strong dehydrated molecular complexes with PS lipids [9–19]. The dehydrated complexes of PS headgroup and calcium ions can even lead to phase separation [9, 10, 14–18]. On the other hand, some studies suggest that the specific binding affinity of Ca^{2+} to negatively charged and zwitterionic phospholipids

is similar, and that the increased cation binding to negatively charged lipid bilayers arises only due to the increased local cation concentration in the membrane vicinity [20, 21]. Dilution of bilayers with PC lipids makes PS headgroups less rigid and reduces their propensity to form strong complexes with multivalent ions [7, 8, 17, 18].

The molecular level interpretation of these observations is, however, lacking, and classical molecular dynamics (MD) simulations have been widely used in efforts to understand the PS headgroup structure, their influence on lipid bilayer properties, and their interaction with ions [19, 22, 34, 49–59]. Unfortunately, the results have depended strongly on the force field used. For example, recent simulations using the NBfix parameters for calcium [60] in CHARMM36 force field [22, 61], combined with 2D infrared spectroscopy, suggest that calcium ions interact only with the carboxylate group of PS lipids [58]; in contrast, the same force field without the NBfix parameters, combined with NMR chemical shifts and REDOR ~~8.Spell out REDOR?~~ experiments, suggests a significant binding affinity also to the phosphate region [59]. On the other hand, simulations with the Berger force field [34, 62], combined with fluorescent and vibrational sum frequency spectroscopy, suggest a significant calcium binding also to the carbonyls in the acyl chains [57].

We have recently demonstrated that such controversies can be resolved by comparing the C–H bond order parameters,

TABLE I: The list of MD simulations of pure PS bilayers without additional salt along with the references to the force fields used and the MD trajectories. Notation $2 \times [\text{time}]$ indicates that two independent MD runs was conducted. Additional simulation details are given in the supplementary information.

| lipid/counter-ions | force field for lipids / ions | $^a N_l$ | $^b N_w$ | $^c T$ (K) | $^d t_{\text{sim}}$ (ns) | $^e t_{\text{anal}}$ (ns) | $^f \text{files}$ |
|----------------------|-------------------------------|----------|----------|------------|--------------------------|---------------------------|-------------------|
| POPS/Na ⁺ | CHARMM36 [22] | 128 | 4480 | 298 | 2×500 | 2×100 | [23] |
| POPS/K ⁺ | CHARMM36 [22] | 128 | 4480 | 298 | 2×500 | 2×100 | [24] |
| POPS/Na ⁺ | CHARMM36ua [?] 2. | 128 | 4480 | 298 | 2×500 | 2×100 | [25] |
| POPS/Na ⁺ | MacRog [26] | 128 | 4480 | 298 | 2×500 | 2×100 | [27] |
| POPS/K ⁺ | MacRog [26] | 128 | 4480 | 298 | 200 | 150 | [28] |
| POPS/Na ⁺ | lipid17 [29] / JC [30] | 128 | 4480 | 298 | 2×600 | 2×100 | [31] |
| POPS/Na ⁺ | lipid17 [29] / ff99 [32] | 128 | 4480 | 298 | 2×600 | 2×100 | [33] |
| POPS/Na ⁺ | Berger [34?]] | 128 | 4480 | 298 | 2×500 | 2×100 | [35] |
| POPS/Na ⁺ | GROMOS-CKPM [?] 3. | 128 | 4480 | 298 | 2×500 | 2×100 | [36] |
| POPS/Na ⁺ | GROMOS-CKP [?] 4. | 128 | 4480 | 298 | 2×500 | 2×100 | [37] |
| POPS/Na ⁺ | Slipids [38] | 128 | 4480 | 298 | 2×500 | 2×100 | [39] |
| DOPS/Na ⁺ | CHARMM36 [22] | 128 | 4480 | 303 | 2×500 | 2×100 | [40] |
| DOPS/Na ⁺ | CHARMM36ua [?] 5. | 128 | 4480 | 303 | 2×500 | 2×100 | [41] |
| DOPS/Na ⁺ | lipid17 [29] / JC [30] | 128 | 4480 | 303 | 2×600 | 2×100 | [42] |
| DOPS/Na ⁺ | lipid17 [29] / ff99 [32] | 128 | 4480 | 303 | 2×600 | 2×100 | [43] |
| DOPS/Na ⁺ | Berger [34?]] | 128 | 4480 | 303 | 2×500 | 2×100 | [44] |
| DOPS/Na ⁺ | GROMOS-CKPM [?] 6. | 128 | 4480 | 303 | 2×500 | 2×100 | [45] |
| DOPS/Na ⁺ | GROMOS-CKP [?] 7. | 128 | 4480 | 303 | 2×500 | 2×100 | [46] |
| DOPS/Na ⁺ | Slipids [38] | 128 | 4480 | 303 | 2×500 | 2×100 | [47] |
| DOPS/Na ⁺ | Slipids [38] | 288 | 11232 | 303 | 200 | 100 | [48] |

^aNumber of lipid molecules with largest mole fraction

^bNumber of water molecules

^cSimulation temperature

^dTotal simulation time

^eTime used for analysis

^fReference for simulation files

S_{CH} , of lipid headgroups between simulations and experiments [63, 64]. The S_{CH} can be directly measured from NMR experiments with high accuracy and compared to simulations in order to evaluate the simulation model quality or to interpret the experiments [65]. Previous studies showed that the structure of PC lipid headgroup and glycerol backbone are not well captured by most MD force fields [63], and that the cation binding to PC lipid bilayers is overestimated [64]. Based on these data, the cation binding affinity to POPC bilayer has since been improved by implicitly including the electronic polarizability using the electronic continuum correction [66]. 9.Should we leave the mention of ECC out from the Introduction (i.e., mention it only in the Conclusions) as the ECC parameters are not used in the paper?

Here, we extend the available set of experimentally measured PS lipid headgroup and glycerol backbone C–H bond order parameters by measuring the signs of the order parameters with S-DROSS solid-state NMR spectroscopy. The quality of headgroup structures and ion binding affinity in the available MD simulation models of PS are then compared with the collected experimental data. The results pave the way

for development of lipid models that correctly describe the headgroup region of negatively charged lipids in physiological salt conditions. Such force fields are expected to be useful in understanding biological function of lipid headgroups and glycerol backbone, as these are known to behave similarly in simple model membranes and in cells [20, 67, 68].

METHODS

Experimental C–H bond order parameters

The headgroup and glycerol backbone C–H bond order parameter magnitudes of 1-palmitoyl-2-oleoyl-*sn*-glycero-3-phospho-L-serine (POPS) were determined by measuring the chemical-shift resolved dipolar splittings with a R-type Proton Detected Local Field (R-PDLF) experiment [90]. The corresponding order parameter signs were measured with a S-DROSS experiment [91] using natural abundance ^{13}C solid state NMR spectroscopy as described previously [92, 93]. The experiments were done in a Bruker Avance III 400 spectrometer operating at a ^1H Larmor frequency of 400.03 MHz. Magic

TABLE II: The list of POPC:POPS mixtures simulated with different molar fractions and different amounts of added calcium. The salt concentrations are calculated as $[\text{salt}] = N_c \times [\text{water}] / N_w$, where $[\text{water}] = 55.5 \text{ M}$. This corresponds the concentration in buffer before solvating lipids, which are reported in the experiments by Roux et al. [17]. Notation $2 \times [\text{time}]$ indicates that two independent MD runs was conducted. The simulation details are given in the supplementary information.

| lipid/counter-ions | force field for lipids / ions | $[\text{CaCl}_2] \text{ (M)}$ | $^a N_l$ | $^b N_w$ | $^c N_c$ | $^d T \text{ (K)}$ | $^e t_{\text{sim}} \text{ (ns)}$ | $^f t_{\text{anal}} \text{ (ns)}$ | $^g \text{files}$ |
|---------------------------------|-------------------------------|-------------------------------|----------|----------|----------|--------------------|----------------------------------|-----------------------------------|-------------------|
| POPC:POPS (5:1)/K ⁺ | CHARMM36 [22, 61] | 0 | 250 | 11207 | 0 | 298 | 200 | 180 | [69] |
| POPC:POPS (5:1)/K ⁺ | CHARMM36 [22, 61] | 0 | 110 | 4620 | 0 | 298 | 2×500 | 2×100 | [70] |
| POPC:POPS (5:1)/Na ⁺ | CHARMM36 [22, 61] | 0 | 110 | 4620 | 0 | 298 | 2×500 | 2×100 | [71] |
| POPC:POPS (5:1) | CHARMM36 [22, 60, 61] | 0.26 | 250 | 11190 | 53 | 298 | 200 | 180 | [72] |
| POPC:POPS (5:1) | CHARMM36 [22, 60, 61] | 1.06 | 250 | 11174 | 214 | 298 | 200 | 180 | [73] |
| POPC:POPS (1:1)/K ⁺ | CHARMM36 [22, 61] | 0 | 150 | 10785 | 0 | 298 | 200 | 180 | [74] |
| POPC:POPS (1:0) | MacRog [26] | 0 | 120 | 5120 | 0 | 298 | 200 | 150 | [75] |
| POPC:POPS (5:1)/K ⁺ | MacRog [26] | 0 | 120 | 5760 | 0 | 298 | 400 | 250 | [76] |
| POPC:POPS (5:1)/K ⁺ | MacRog [26] | 0.10 | 120 | 5760 | 10 | 298 | 600 | 300 | [76] |
| POPC:POPS (5:1)/K ⁺ | MacRog [26] | 0.30 | 120 | 5760 | 31 | 298 | 600 | 300 | [76] |
| POPC:POPS (5:1)/K ⁺ | MacRog [26] | 1.00 | 120 | 5760 | 104 | 298 | 600 | 300 | [76] |
| POPC:POPS (5:1)/K ⁺ | MacRog [26] | 3.00 | 120 | 5760 | 311 | 298 | 600 | 300 | [76] |
| POPC:POPS (5:1)/K ⁺ | Lipid14/17 [29, 77] | 0 | 120 | 5760 | 0 | 298 | 2×500 | 2×200 | [78] |
| POPC:POPS (5:1)/Na ⁺ | Lipid14/17 [29, 77] | 0 | 120 | 5760 | 0 | 298 | 2×500 | 2×200 | [79] |
| POPC:POPS (5:1) | Lipid14/17 [29, 77] | 0.50 | 120 | 5760 | 52 | 298 | 2×500 | 2×200 | [80] |
| POPC:POPS (5:1) | Lipid14/17 [29, 77] | 1.00 | 120 | 5760 | 104 | 298 | 2×500 | 2×200 | [80] |
| POPC:POPS (5:1) | Lipid14/17 [29, 77] | 2.00 | 120 | 5760 | 208 | 298 | 2×500 | 2×200 | [80] |
| POPC:POPS (5:1) | Lipid14/17 [29, 77] | 3.00 | 120 | 5760 | 311 | 298 | 2×500 | 2×200 | [80] |
| POPC:POPS (5:1) | Lipid14/17 [29, 77] | 4.00 | 120 | 5760 | 415 | 298 | 2×500 | 2×200 | [80] |
| POPC:POPS (5:1)/Na ⁺ | Lipid14/17 [29, 77] | 0 | 60 | 3600 | 0 | 298 | 1000 | 1000 | [81] |
| POPC:POPS (5:1)/Na ⁺ | Lipid14/17 [29, 77, 82, 83] | 0.08 | 60 | 3561 | 5 | 298 | 1000 | 1000 | [81] |
| POPC:POPS (5:1)/Na ⁺ | Lipid14/17 [29, 77, 82, 83] | 0.13 | 60 | 3561 | 8 | 298 | 1000 | 1000 | [81] |
| POPC:POPS (5:1)/Na ⁺ | Lipid14/17 [29, 77, 82, 83] | 0.20 | 60 | 3561 | 13 | 298 | 1000 | 1000 | [81] |
| POPC:POPS (5:1)/Na ⁺ | Lipid14/17 [29, 77, 82, 83] | 0.41 | 60 | 3522 | 26 | 298 | 1000 | 1000 | [81] |
| POPC:POPS (5:1)/Na ⁺ | Lipid14/17 [29, 77, 82, 83] | 0.62 | 60 | 3483 | 39 | 298 | 1000 | 1000 | [81] |
| POPC:POPS (4:1)/Na ⁺ | Berger [34, 84] | 0 | 102 | 4290 | 0 | 310 | 120 | 80 | [85] |
| POPC:POPS (4:1) | Berger [34, 84] | 0.102^h | 104 | 4306 | 24 | 310 | 300 | 100 | [86] |
| POPC:POPS (4:1) | Berger [34, 84] | 0.715^h | 104 | 4306 | 72 | 310 | 300 | 100 | [87] |
| POPC:POPS (5:1)/Na ⁺ | GROMOS-CKP [?]] | 0 | 110 | ? | 0 | 298 | 2×500 | 2×100 | [88] |
| POPC:POPS (5:1)/Na ⁺ | GROMOS-CKPM [?]] | 0 | 110 | ? | 0 | 298 | 2×500 | 2×100 | [89] |

^aNumber of POPC molecules

^bNumber of water molecules

^cNumber of additional cations

^dSimulation temperature

^eTotal simulation time

^fTime used for analysis

^gReference for simulation files

^hCalculation of concentration complicated by the usage scaled ions. Concentration taken as reported in the delivered data.

angle spinning (MAS) of the sample was used at a frequency of 5.15 kHz (R-PDLF experiment) and 5 kHz (S-DROSS experiment). The following experimental setups were used.

C–H bond order parameters from the R-PDLF experiment.

The parameters are described according to Figures 1c and 2c of the original reference for the R-PDLF experiment [90]. The refocused-INEPT delays were $\tau_1 = 1.94 \text{ ms}$ and $\tau_2 = 0.97 \text{ ms}$.

The used radio frequency pulses had the following nutation frequencies: 46.35 kHz (R18₁⁷ pulses), 63.45 kHz (¹³C 90° and 180°), 50 kHz (SPINAL64 ¹H decoupling pulses). The t_1 increment was equal to $10.79 \mu\text{s} \times 18 \times 2$, and 32 points in the indirect dimension were recorded using 1024 scans for each, with a recycle delay of 5 s and a spectral width of 149.5 ppm.

Order parameter signs from the S-DROSS experiment. The

parameters are described according to Figures 1b and 1c of the original reference for the S-DROSS experiment [91]. The refocused-INEPT delay δ_2 was 1.19 ms. The τ_1 and τ_2 in the S-DROSS recoupling blocks R were set as $\tau_1 = 39.4 \mu\text{s}$ and $\tau_2 = 89.4 \mu\text{s}$. The used radio frequency pulses had the nutation frequencies: 63.45 kHz (^{13}C 90° and 180°), 50 kHz (^1H SPINAL64 decoupling). The t_1 increment (dipolar recoupling dimension) was 800 μs , and a total of 8 points along t_1 were measured using 1024 scans for each, with a recycle delay of 5 s and a spectral width of 149.5 ppm.

Numerical simulations of S-DROSS curves. The numerical simulations of S-DROSS curves were performed using the SIMPSON simulation package [94] by inputting the ^{13}C - ^1H dipolar couplings, either as determined by the R-PDLF experiments, or as calculated from the known ^2H quadrupolar couplings [7]. The chemical shift anisotropy and homonuclear couplings were neglected, and the input file *rep2000*^{10.citation needed?} was used to simulate a random distribution of bilayer orientations in the samples studied.

Sample preparation. The sample was prepared simply by mixing POPS (1-palmitoyl-2-oleoyl-*sn*-glycero-3-phospho-L-serine, purchased from Avanti Polar Lipids as sodium salt) with water (lipid:water 60:40 wt-%) in an Eppendorf tube by mixing and centrifuging the sample repeatedly until a homogeneous viscous fluid was obtained ^{11.How long and how many repeats did this take approximately? Was the homogeneity determined visually?.} Then 20 mg of the sample was transferred to an NMR insert suitable for 4 mm NMR rotors.

Molecular dynamics simulations

Molecular dynamics simulation data were collected using the Open Collaboration method [63], with the NMRLipids Project blog (nmrlipids.blogspot.fi) and GitHub repository (github.com/NMRLipids/NMRLipidsIVotherHGs) as the communication platforms. The simulated systems are listed in Tables I (pure PS bilayers without additional ions) and II (mixed PC:PS bilayers at various salt concentrations). Further simulation details are given in the SI, and the simulation data are indexed in a searchable database available at www.nmrlipids.fi, and in the NMRLipids/MATCH repository (github.com/NMRLipids/MATCH).

The C-H bond order parameters were calculated directly from the carbon and hydrogen positions using the definition

$$S_{\text{CH}} = \frac{1}{2} \langle 3 \cos^2 \theta - 1 \rangle, \quad (1)$$

where θ is the angle between the C-H bond and the membrane normal (taken to align with z , with bilayer periodicity in the xy -plane). Angular brackets denote average over all sampled configurations. The order parameters were first calculated averaging over time separately for each lipid in the system. The average and the standard error of the mean were then calculated over different lipids. Python program

(`scripts/calcOrderParameters.py`) that uses the MDAnalysis library [95, 96] is available in Ref. 97. The ion ^{12.There are ion number densities, right?} number density profiles were calculated using the `gmxdensity` tool of the Gromacs software package [98].

Comparison of ion binding to negatively charged lipid bilayers between simulations and experiments using the molecular electrometer concept

The order parameters of the α and β carbons in the PC headgroup decrease proportionally to the amount of positive charge bound to the bilayer [99–101], and can therefore be used to measure the ion binding affinity. This concept, known as the molecular electrometer, is especially useful for comparison between simulations and experiments, as the headgroup order parameters at varying cation concentrations can be easily calculated from simulations and compared to experimental data [64]. The headgroup order parameters of negatively charged PS and PG lipids also exhibit systematic, but less understood dependencies on the bound charge [17, 102–104]. Therefore, measuring the PC headgroup order parameters from mixed (here PS:PC) bilayers [17, 18, 104] (see SI section S2 provides a more straightforward way of characterizing the ion binding to negatively charged membranes.

Important preliminary step for using the molecular electrometer concept is to calibrate the PC order parameter response to a known amount of bound charge [64, 66]. This can be done using experimental data from mixtures of monovalent cationic surfactants (dihexadecyldimethylammonium) and POPC [66, 105], (see SI section S3). Additionally, we quantify the response of PC headgroup order parameters to the negatively charged PS, which also follows the molecular electrometer concept in experiments [68] (see SI section S2).

Studies applying the molecular electrometer concept have utilized two different definitions for salt concentration: The concentrations are reported either in water before solvating the lipids [17, 64, 99], or in bulk water after solvating the lipids [66, 100]. In this work, we use the former definition to be consistent with the reference experimental data [17]. However, the choice of definition has only a marginal effect to the results in simulations with realistic ion binding affinity (see SI section S4).

RESULTS AND DISCUSSION

Headgroup and glycerol backbone order parameters of POPS from ^{13}C NMR

The INEPT and 2D R-PDLF experiments from POPS sample give well resolved spectra for all the carbons in the headgroup and glycerol backbone regions (Fig. 1). The glycerol backbone carbon peaks were assigned according to the POPC spectra [92]. The peaks for β and α carbons were assigned

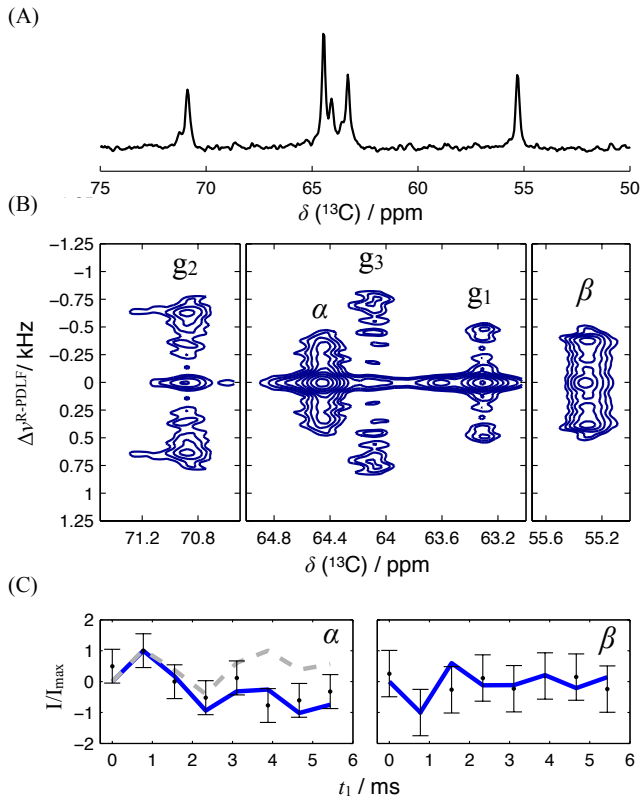


FIG. 1: The headgroup and glycerol backbone region of the (A) IN-EPT spectrum and (B) 2D R-PDLF spectra. (C) Experimental S-DROSS data (points), and SIMPSON simulations (blue lines) with the C—H bond order parameter values of -0.12 for the β -carbon, and +0.09 and -0.02 for the α -carbon. Dashed gray line is the S-DROSS curve from a SIMPSON simulation with a positive value (+0.02) for the smaller α -carbon C—H bond order parameter.

13.I think that the peak labeling would be good to show also in (A).

according to the known order parameters from the ^2H NMR experiments [7]. Slices of the R-PDLF spectra and the resulting order parameter values are shown in the supplementary information (Fig. S6).

Since the R-PDLF and previous ^2H NMR experiments [7, 18] give only the absolute values of order parameters, we determined the signs of the PS headgroup order parameters using the S-DROSS experiment [91]. For a given carbon, its S-DROSS dipolar modulation profile in the indirect dimension is a superposition of sinusoidal functions from the possible orientations of crystallites in the sample (or bilayer patches). We phase corrected the 2D spectrum in the direct dimension such that positive and negative signs for the C—H bond order parameter give rise to profiles that initially increase and decrease, respectively. In practice, it is useful to use the known negative sign of the acyl chain carbons as a reference to perform the phase correction and interpret the distinct initial slopes of the S-DROSS profiles as shown in figure 1. The S-DROSS slice for the β -carbon clearly shows an initial decrease and therefore its order parameter must be negative. For

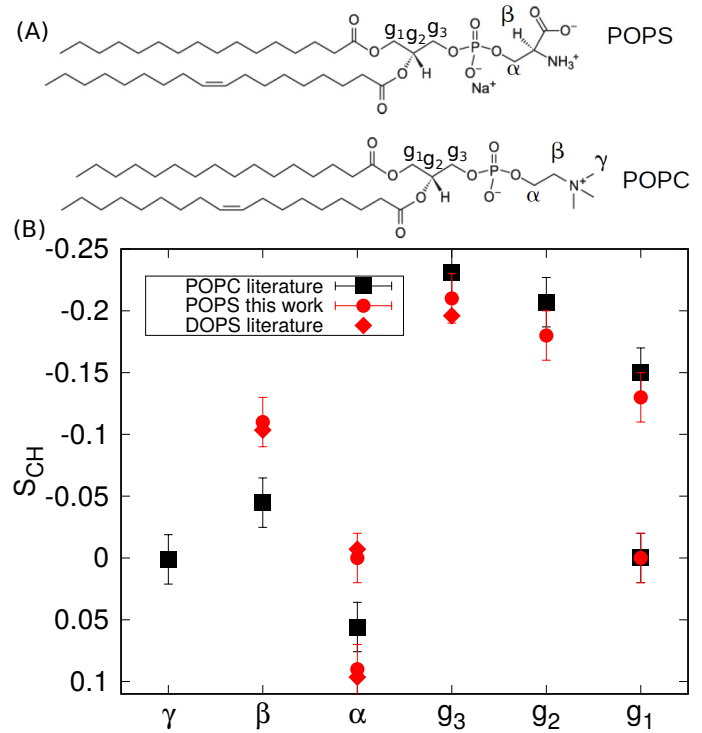


FIG. 2: (A) Chemical structures and labels for the headgroup and glycerol backbone carbons. (B) Headgroup and glycerol backbone order parameters of POPC ($T = 298 \text{ K}$) measured in this work compared with the previously published values from DOPS ($T = 303 \text{ K}$, ^2H NMR, 0.1M of NaCl) [7] and POPC ($T = 300 \text{ K}$, ^{13}C NMR) [92] experiments. Signs of the PS order parameters are measured in this work whereas signs of the PC order parameters are measured previously [93]. The size of errorbars (± 0.02) shown for ^{13}C NMR data is justified previously [63, 65].

14.Replace the "literature" with "from Ref X" has been suggested

<https://github.com/NMRLipids/NMRLipidsIVotherHGs/issues/34>. We can do this just before submission when citation numbers will not change anymore.

the α -carbon such analysis is not as trivial due to the two inequivalent order parameters of the two distinct C—H bonds. However, the beginning of its S-DROSS slice suggests that the larger order parameter of the alpha-carbon is positive and the decrease towards negative values at longer t_1 suggests that the smaller order parameter is negative. This is confirmed by a SIMPSON simulation using the value of -0.02 from ^2H NMR experiment [18] for the smaller order parameter. The literature value was used because the resolution of our R-PDLF experiment was not sufficient to determine the small value of the order parameter. The S-DROSS curve from SIMPSON simulation with a positive value for the smaller order parameter (dashed grey in Fig. 1 C)) did not agree with the experiment, corroborating the interpretation that the smaller order parameter is negative.

The headgroup and glycerol backbone order parameters of POPC measured in this work are in good agreement with the previously reported values from ^2H NMR experiments of DOPS [7] (Fig. 2). When compared with the previously

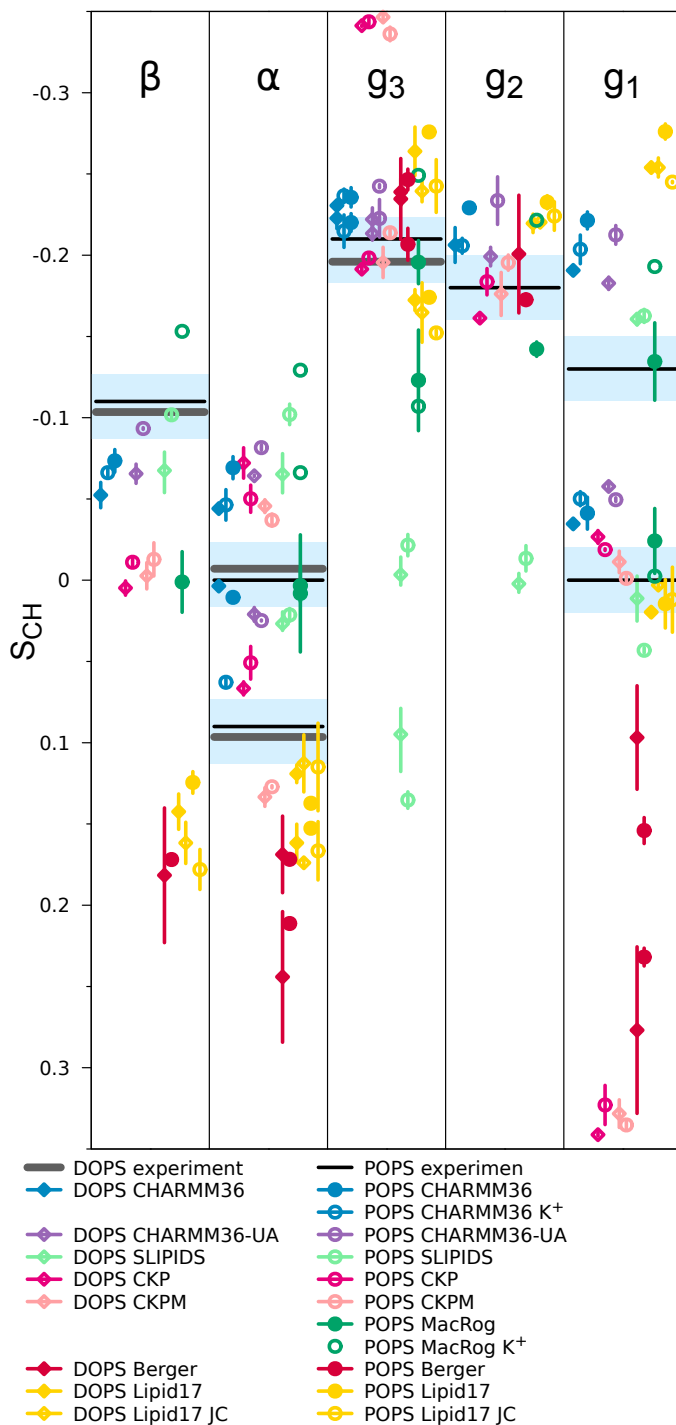


FIG. 3: Order parameters of PS headgroup (β and α) and glycerol backbone (g_3 , g_2 , g_1) from NMR experiments (horizontal lines), and MD simulations with different force fields (symbols). Experimental data for DOPS are measured with 0.1 M of NaCl [7], while all the other data are without additional salt. The data for DOPS is at 303 K and the data for POPS is at 298 K. Light blue areas span 0.04 units around the average of the extremal experimental values, in accordance with the expected quantitative accuracy of experiments [65]. The vertical bars shown for all simulation values (excl. MacRog K^+) are not error bars, but demonstrate that for these systems we had at least two data sets; the ends of the bars mark the extreme values from the sets, and the dot marks their measurement-time-weighted average.

measured values for POPC [92] (Fig. 2), the β -carbon order parameter is significantly more negative and α -carbon experiences a significant forking (different order parameters for the two hydrogens in the same carbon [65]) in the PS headgroup. These features have been interpreted to arise from a rigid PS headgroup conformation, stabilized by hydrogen bonds or electrostatic interactions [7, 8], but detailed structural interpretation is not available.

We note that the the DOPS 2H NMR reference data found in the literature [7, 17] was obtained by first solvating the lipids with a buffer solution and then centrifuging the sample to a pellet that was used for the measurements. Such samples have a lower lipid concentration (approximately 10 wt % of lipids [7, 17, 106]) than gravimetric samples (60 wt %) and simulations (approximately 50-60 wt %) in this work. Larger multilamellar repeat distances are expected in the samples with lower lipid concentrations due to the swelling caused by electrostatic repulsion in pure PS lipid systems [107]. Yet the PS headgroup order parameters measured from gravimetric samples (POPS) in this work are in good agreement with the results from centrifuged samples [7]. This, together with the rapid decrease of equilibrium repeat distance with addition of monovalent salt [107, 108], indicates that the hydration levels of multilamellae are sufficiently similar in the simulations and reference experiments.

Headgroup and glycerol backbone in simulations of PS lipid bilayers without additional ions

The different PS MD models produce a wide variety of headgroup and glycerol backbone order parameters (Fig. 3) and structures (Fig. S9) between different simulation models, as previously observed also for PC lipids [63]. None of the models produces a set of order parameters in full agreement with the experiments. The models perform generally less well for PS than for PC (Figs. 3 and 5 vs. Figs. 2 and 4 in Ref. [63]). which complicates the interpretation of structural differences between PC and PS headgroups.

However, concentrating on the headgroup, we see that the best performing models (Slipids, CHARMM36 and CHARMM36ua) do replicate the larger-than-in-PC forking of the α -carbon **17. observed in the experiments?** and the Slipids force field additionally correctly produces the significantly smaller β -carbon order parameter for PS compared to PC (Fig. 3 vs. Fig. 2 in Ref. 63) **18. refer to experiments also?**

Interestingly, the three models that best fit the experimental data have a narrower distribution in the $C_\alpha-C_\beta-C_\gamma-O_\gamma$ dihedral angle (single peak around 120°) in comparison to the other models which yield a distribution between two angles (Fig. S7). The restricted motion is also visible in the sampled conformations (Figs. 4 (A) and S9) suggesting that the rotation of the carboxyl group is limited in the serine headgroup. In addition, the $N-C_\beta-C_\alpha-O_\alpha$ dihedral exhibits a more asymmetric and restricted **19. rather: narrow?** angle distribution for PS than for PC headgroup in CHARMM36 simulations

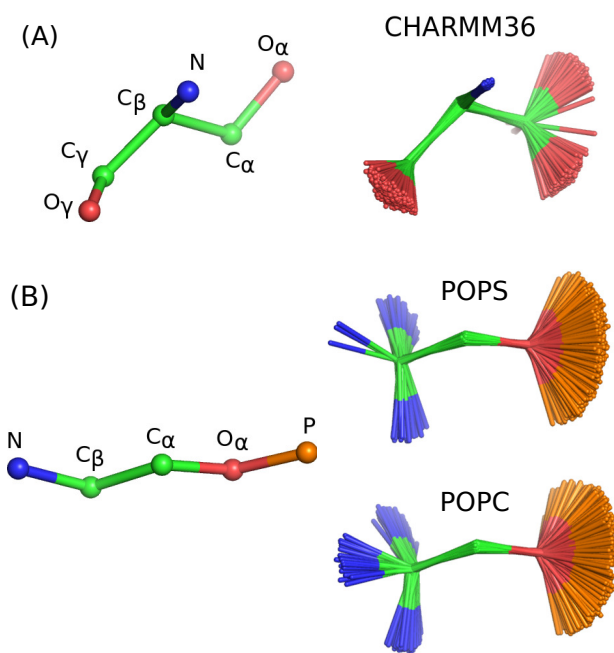


FIG. 4: Overlaid snapshots from simulations conducted with CHARMM36 — the force field producing the best agreement with experiments — demonstrate the conformational fluctuations around (A) $C_\alpha-C_\beta-C_\gamma-O_\gamma$ and $O_\alpha-C_\alpha-C_\beta-N$ of PS headgroup and (B) $N-C_\beta-C_\alpha-O_\alpha$ and $C_\beta-C_\alpha-O_\alpha-P$ dihedrals of PS and PC headgroups. The publicly available trajectories via Zenodo were used for CHARMM36 POPC and Slipids POPC (Refs. 109 and 110, respectively).

15. Figure clarity is questioned in:

<https://github.com/NMRLipids/NMRLipidsIVotherHGs/issues/48>

that have the best agreement with experiments (Figs. 4 (B) and S10). The results might reflect the increased rigidity anticipated²⁰ detected, predicted, speculated? in the early experimental studies [7, 8].

The suggested characteristic conformations of the PS headgroup can be useful when interpreting experiments. However, as the none of the tested models fully reproduces the experimental order parameters, more accurate MD force fields are required to confirm the correct conformational ensemble.

Counterion binding and interactions between PC and PS headgroups

Membranes containing PS lipids are always accompanied with counterions that modulate electrostatic interactions between lipids and other biomolecules. MD simulations have suggested that counterions reduce the area per lipid of PS bilayers to be smaller than in PC bilayers [34, 50, 51] by screening the repulsion between charged lipid headgroups. Counterion density profiles along membrane normal show significant differences between force fields in both binding affinity and distribution of ions in the interface (Fig. 6). The experimen-

| | β | α | g_3 | g_2 | g_1 | Σ |
|--------------|---------|----------------|----------------|-------|----------------|----------|
| CHARMM 36 K+ | M | M | M _F | M | M _F | 7 |
| CHARMM 36 | M | M _F | M | M | M _F | 8 |
| CHARMM 36-UA | M | M | M | M | M _F | 9 |
| MacRog K+ | M | M _F | M _F | M | M _F | 11 |
| MacRog | M | M _F | M _F | M | M | 14 |
| GROMOS-CKP | M | M _F | M _F | | M _F | 14 |
| GROMOS-CKPM | M | M _F | M _F | | M _F | 14 |
| Berger | M | M _F | M _F | | M _F | 14 |
| Slipid | M | M | M _F | M | M _F | 14 |
| Lipid17 | M | M _F | M _F | M | M _F | 18 |
| Lipid17 JC | M | M _F | M _F | M | M _F | 18 |

FIG. 5: Rough subjective ranking of force fields based on Figure 3. Here \bar{O} indicates a magnitude problem, \bar{O} a forking problem; letter size increases with problem severity. Color scheme: \bar{O} within experimental error (dark green), \bar{O} almost within experimental error (light green), \bar{O} clear deviation from experiments (light red), and \bar{O} major deviation from experiments (dark red). The Σ -column shows the total deviation of the force field, when individual carbons are given weights of 0 (matches experiment), 1, 2, and 4 (major deviation). For full details of the assessment, see Supplementary Information.

tal area per lipid ($62.7 \pm 1.3 \text{ \AA}^2$) [55] is reproduced only in Gromos-CKP and in the MacRog simulation with potassium counterions, while other models give considerably smaller areas (Fig. 6). However, the counterion binding and the concomitant electrostatic screening of the headgroup repulsion does not fully explain the low area per molecule values. since the MacRog simulation, which has the strongest sodium binding (the lowest concentrations in bulk water), gives the same area per molecule as the CHARMM36ua simulation, which has significantly weaker counterion binding affinity. On the other hand, MacRog simulations with potassium produce a

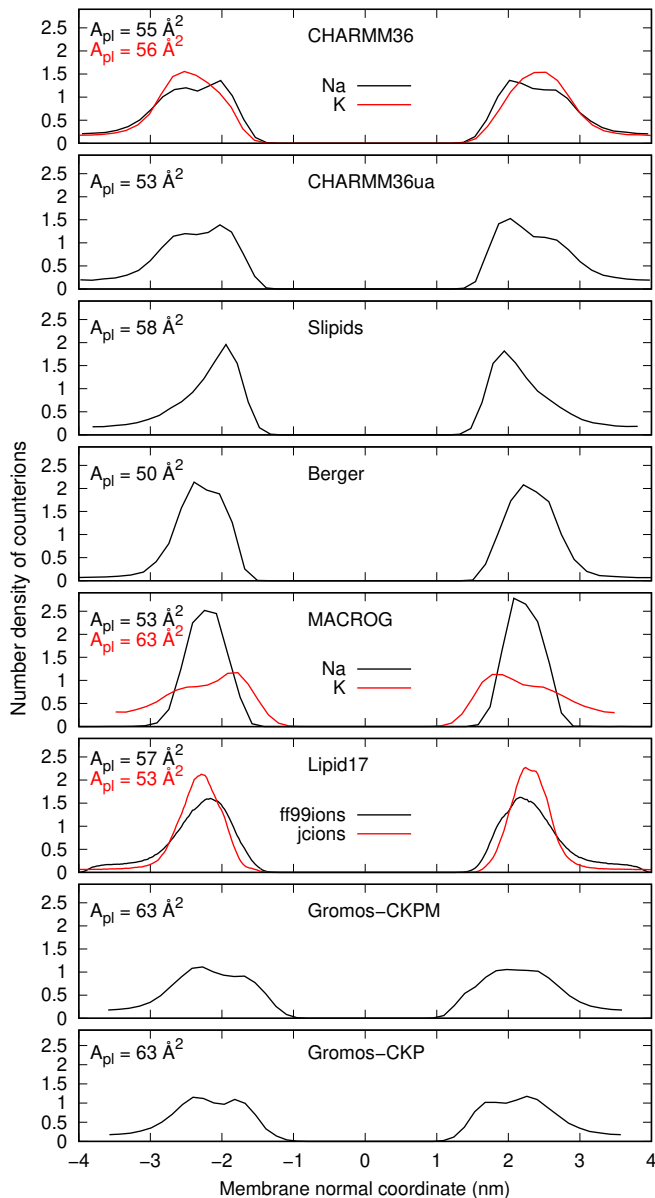


FIG. 6: Counterion density profiles along the membrane normal and areas per lipid (A_{pl}) of POPS lipid bilayer from simulations with different force fields. The experimental area per lipid is $62.7 \pm 1.3 \text{ Å}^2$ [55].

16. Commented by M. Javanainen in blog: MacRog pure POPS is simulated with Verlet cutoff scheme, Piggot is rerunning with group cutoff scheme. Check if affects results & update figures when ready

larger area per molecule (63 Å^2) than with sodium (53 Å^2) in line with the weaker potassium binding affinity (Fig. 6). In conclusion, the results are in line with the previous study suggesting that the low areas per molecule in PS lipid bilayers originate from the combination of both counterion binding and hydrogen bonding network between lipid headgroups [111]. 22. can we really say this based on our data? We don't discuss hydrogen

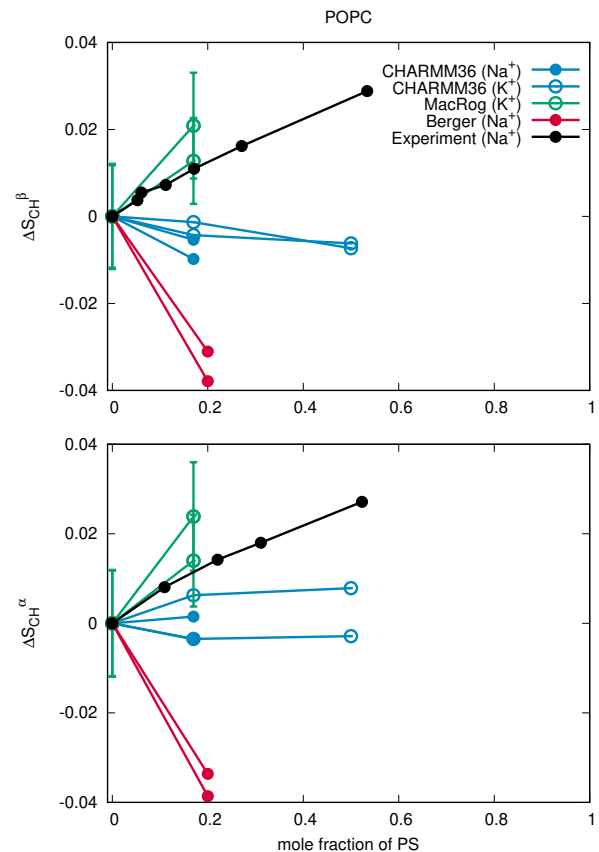


FIG. 7: Changes of POPC headgroup order parameters with increasing amount of POPS in POPC:POPS mixtures at 298 K. Experimental values are from Ref. 68 with the signs measured in Ref. 93.

21. After we know which force field is used for POPC in Gromos-CKP simulations, we might be able to add Gromos-CKP data into this plot.

bonding

The experimentally observed modulation of headgroup order parameters by increasing salt concentration (the molecular electrometer concept) has been previously used to evaluate the cation binding to zwitterionic PC bilayers in simulations [64]. Studying binding of cations to negatively charged lipid bilayers is less straightforward due to the presence of cationic counterions and the lack of a ion-free reference state. The analysis is further complicated by the artificial aggregation of counterions observed in some simulations (section S7 in the SI). 23. Why isn't this a problem with PC. Therefore, we evaluate here the amount of bound charge not by adding salt (although also this is discussed in the SI section S7), but by studying the changes of the headgroup order parameters with increasing amount of negatively charged lipids (and thus increasing amount of cationic counterions) in the bilayer.

According to the molecular electrometer concept, the headgroup order parameters of POPC increase when negatively charged POPS lipids are incorporated in lipid bilayer (section S1) [68, 101]. This is reproduced in the MacRog simulations with potassium counterions (Fig. 7), which have the

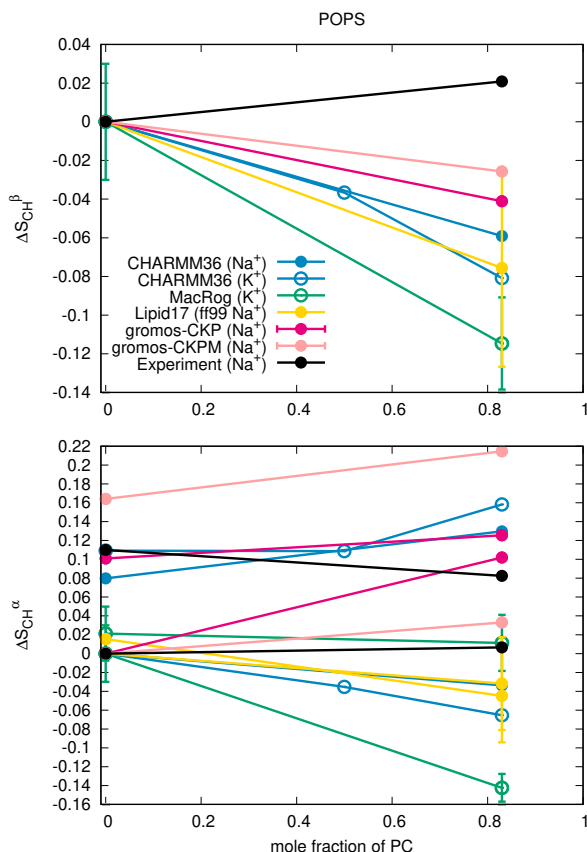


FIG. 8: Modulation of POPS headgroup order parameters with increasing amount of POPC in POPC:POPS mixtures at 298 K. Experimental values with the signs are measured for pure POPS system in this work. The signs are assumed to be the same for the mixture and the values are from Ref. 17. The y-axis for the α -carbon results of POPS (bottom) is transferred with the same value for both order parameters such that the lower order parameter value from pure POPS is at zero to correctly illustrate the significant forking.

weakest binding affinity to POPS lipid bilayers (Fig. 6). The CHARMM36 and Berger simulations either exhibit no change or show a decrease in the POPC headgroup order parameters as the amount of POPS increases (Fig. 7). This can be explained by the stronger counterion binding affinity, which cancels the effect of negatively charged headgroups and prevents the experimentally observed increase of headgroup order parameters with growing amount of PS lipids. Therefore, we suggest that the relatively weak binding of potassium in the MacRog simulations (Fig. 6) produces the most realistic surface charge density in membranes containing PS lipids, while the other tested simulation models overestimate the counterion binding affinity. The results are in line with the behaviour of headgroup order parameters as a function of added counterions analyzed in section S7 in the SI.

The reduced forking of the POPS α -carbon (Fig. 8) together with other experimental results suggest less rigid structure of PS headgroups when diluted with POPC [7, 8, 17, 18, 68]. Unfortunately, none of the tested models correctly reproduce

the modulation of POPS headgroup order parameters with increasing amount of POPC in POPC:POPS mixtures (Fig. 8). and we conclude that more accurate force fields are needed to correctly describe the PC-PS headgroup interactions in MD simulations.

Ca^{2+} binding affinity to bilayers with negatively charged PS lipids

Calcium binding affinity to membranes containing the negatively charged PS lipids can be experimentally measured by detecting the PC lipid headgroup order parameters from POPC:POPS (5:1) mixtures (section S2), where the measurement is not complicated by the dehydrated lipid-ion complexes and phase separation and the bilayer remains uniform [15–18]. Despite the lack of an ion-free reference state in the presence of negatively charged lipids, our simulations give coherent results for POPC headgroup order parameters as a function of CaCl_2 in the POPC:POPS (5:1) mixtures (Fig. 9). As expected from the previous study of pure PC lipid bilayers [64], almost all the tested simulation models overestimate the experimentally observed [17] decrease of the POPC headgroup order parameters in POPC:POPS (5:1) mixtures as Ca^{2+} concentration increases (Fig. 9), indicating overestimated calcium binding affinity. The only exception is the CHARMM36 model with the NBfix interaction employed for calcium [60], which underestimates the modulation of order parameters, indicating weaker binding affinity than experiments. Notably, CHARMM36 simulations with the NBfix corrections [22, 60] give similar binding affinities of calcium and sodium to POPC bilayer (see section S8), in contrast to the experiments [99, 100, 113]. Therefore, we conclude that the calcium binding affinity is underestimated in CHARMM36 simulations when using the NBfix for calcium [60], but overestimated in all the other tested models. This is evident in the calcium density distributions where almost all Ca^{2+} ions bind to the membrane interface in all simulation models except CHARMM36 (Fig. 10).

Experimentally, the POPS headgroup order parameters in POPC:POPS (5:1) mixtures exhibit a strong dependence of CaCl_2 with small concentrations and rapid saturation below 100 mM (Fig. 9). The β -carbon order parameter increases with added CaCl_2 , whereas the larger α -carbon order parameter decreases; a slight increase is observed in the smaller α -carbon. All these changes are significantly overestimated in the tested simulation models, including CHARMM36 which underestimated the binding affinity. Importantly, the different simulation models predict qualitatively different behaviour for the POPS α -carbon order parameters with added calcium. For example, both order parameters decrease in Berger, but increase in MacRog, and in Lipid14/17 and CHARMM36 a more complicated behavior is seen. This is in contrast to the PC headgroup, where qualitatively correct response to bound ions is observed in all simulation models, despite significant discrepancies in the headgroup structure without additional ions [64].

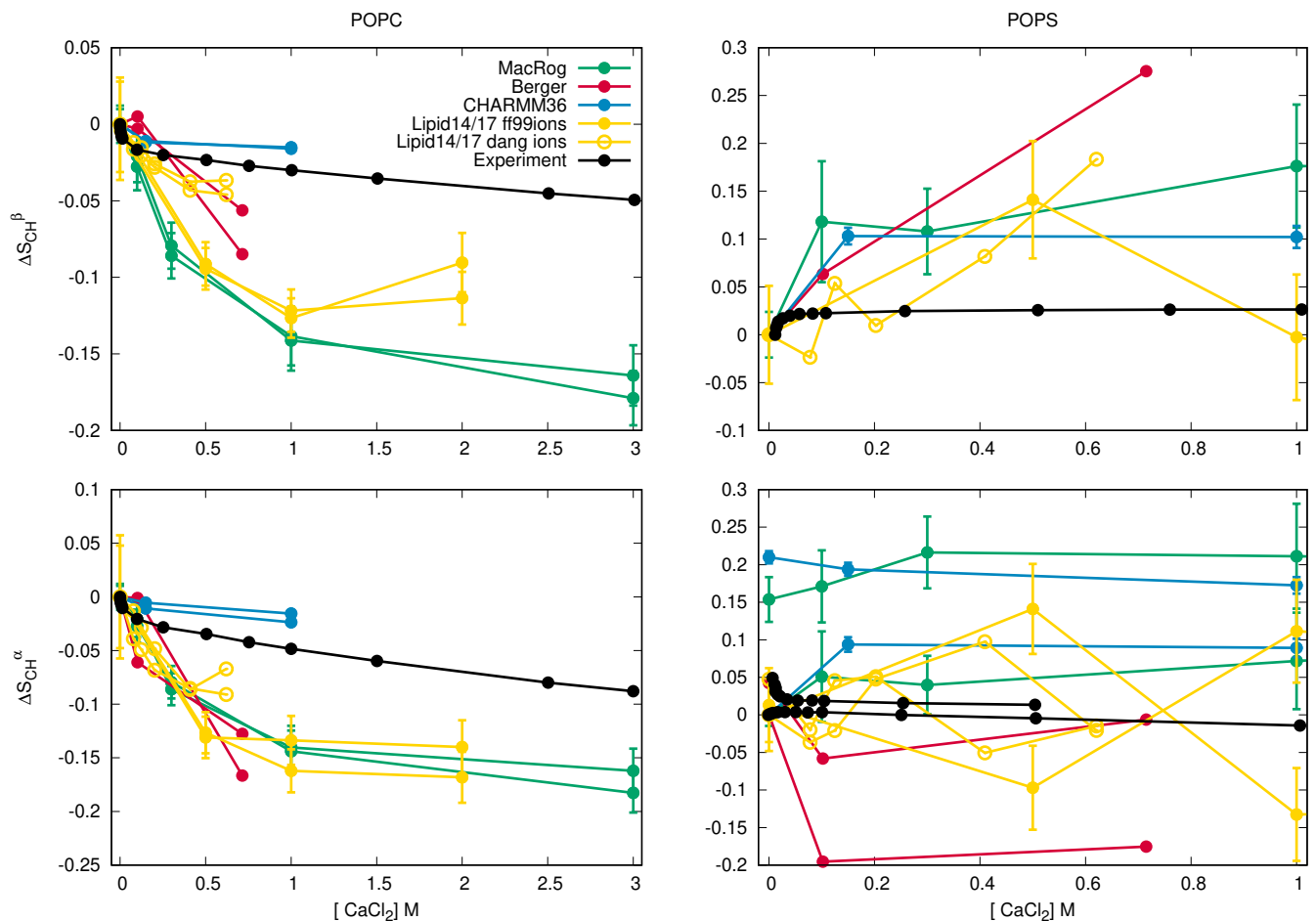


FIG. 9: Variation of POPC (left) and POPS (right) headgroup order parameters from POPC:POPS (5:1) mixture as a function CaCl_2 concentration from experiments [17] and different simulations at 298K (except the data for Berger model is from simulation of POPC:POPS (4:1) mixture at 310K [57, 112]). The order parameter values from systems without calcium are set as the zero point of y-axis, except for the α -carbon order parameter of POPS (bottom, right) for which both order parameters are shifted such that the lower order parameter is zero without additional ions. This is to correctly illustrate the forking with different concentrations of calcium. Potassium counterions are used in MacRog simulations and sodium counterions in Lipid14/17 simulations. In CHARMM36 and Berger simulation with added calcium, the charge is neutralized with calcium and monovalent counterions are not present.

Therefore, we conclude that improvement of force fields is necessary to correctly capture the interactions between the PS headgroup and calcium ions in MD simulations.

CONCLUSIONS

Lipids with PS headgroups, and their interactions with ions, play an important role in lipid-mediated signaling processes [2, 4]. Attempts to use MD simulations to interpret the spectroscopic data have produced contradictory results for the calcium binding details to PS headgroups [57–59]. Here (as was previously done for PC lipids [63, 64]) we used the headgroup C–H bond order parameters and the open collaboration approach to evaluate the quality of the headgroup structure and ion binding affinity to PS lipids in available MD force fields.

The main advantage of this approach is the direct connection between the accurately measured experimental order parameters and the simulations, which reduces the ambiguity in the interpretation of experiments.

First, we complemented the available experimental data [7, 17] by measuring the signs of the PS headgroup order parameters. Comparison to these data revealed that none of the available force fields reproduce the PS headgroup order parameters within the experimental accuracy. However, the best models for the serine headgroup suggested a characteristic rigid conformation for its carboxyl group. Comparison to the experimentally observed order parameters in POPC:POPS (5:1) bilayers at varying ion concentrations [17] then showed that the tested MD force fields overestimate the cation binding affinity to these bilayers with two exceptions. 1) The MacRog simulation with potassium counterion appear to pro-

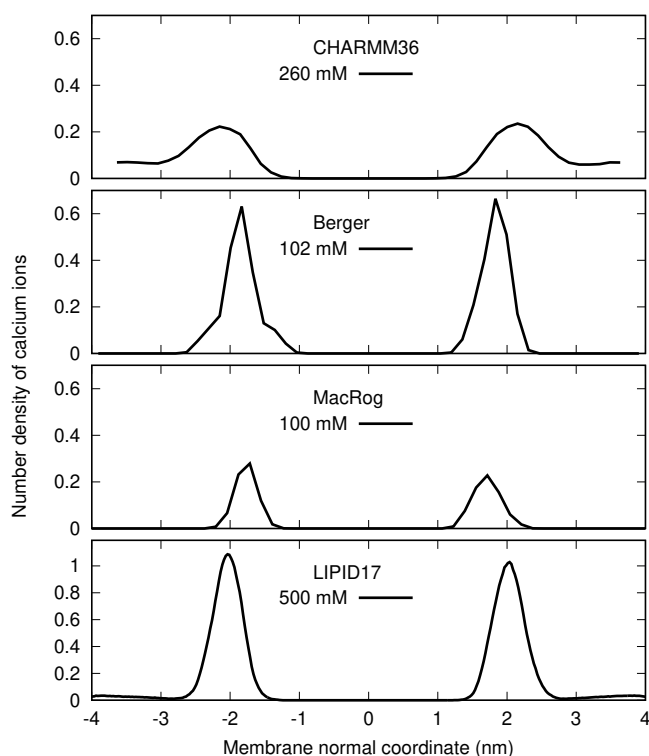


FIG. 10: Number density profiles of Ca^{2+} from POPC:POPS (5:1) mixtures simulated with different force fields. The smallest simulated CaCl_2 concentrations are shown. The density profiles for all the simulated concentrations are given in SI figure S18.

24. Should we include also counterions into the plot?

duce the most realistic monovalent ion binding affinity to PS-containing lipid bilayers. 2) The CHARMM36 force field with the recently introduced NBfix correction for calcium [60] underestimated the calcium binding affinity. The experimentally measured response of the PS headgroup order parameter to the bound calcium, and to the dilution of bilayer with zwitterionic PC lipids, were not qualitatively reproduced in any of the tested force fields, which underlines the need for more accurate the MD force fields to study interactions between PS lipids and other biomolecules. This is in contrast to the previous results with PC lipids, where the experimentally measured headgroup order parameter responses to the bound charge were in qualitative agreement even though the headgroup structures themselves were incorrect and the cation binding affinities overestimated [64].

Our results pave the way for the development of better MD force fields for PS lipids. Using the headgroup order parameters, we were able to evaluate the quality of various conformational ensembles in different force fields. This can guide the development of force fields that would correctly reproduce the conformations sampled by PS headgroups. The experimental dataset of headgroup order parameters from POPC:POPS (5:1) mixture with different cation concentrations can be used to improve cation binding details in the force fields, as re-

cently demonstrated for POPC using the electronic continuum correction [66]. Similar study for POPS is being progressed separately [114].

OHSSO acknowledges financial support from Academy of Finland (315596), Integrated Structural Biology Research Infrastructure of Helsinki Institute of Life Science (Instruct-HiLIFE), and CSC-IT center for science for computational resources. MJ acknowledges financial support from the Emil Aaltonen foundation and CSC-IT center for science for computational resources.

* samuli.ollila@helsinki.fi

- [1] M. A. Lemmon, *Nat. Rev. Mol. Cell Biol.* **9**, 99 (2008).
- [2] P. A. Leventis and S. Grinstein, *Annual Review of Biophysics* **39**, 407 (2010).
- [3] L. Li, X. Shi, X. Guo, H. Li, and C. Xu, *Trends in Biochemical Sciences* **39**, 130 (2014), ISSN 0968-0004.
- [4] T. Yeung, G. E. Gilbert, J. Shi, J. Silvius, A. Kapus, and S. Grinstein, *Science* **319**, 210 (2008).
- [5] H. Zhao, E. K. J. Tuominen, and P. K. J. Kinnunen, *Biochemistry* **43**, 10302 (2004).
- [6] G. P. Gorbenko and P. K. Kinnunen, *Chemistry and Physics of Lipids* **141**, 72 (2006).
- [7] J. L. Browning and J. Seelig, *Biochemistry* **19**, 1262 (1980).
- [8] G. Büldt and R. Wohlgemuth, *The Journal of Membrane Biology* **58**, 81 (1981), ISSN 1432-1424, URL <http://dx.doi.org/10.1007/BF01870972>.
- [9] H. Hauser, E. Finer, and A. Darke, *Biochemical and Biophysical Research Communications* **76**, 267 (1977), ISSN 0006-291X, URL <http://www.sciencedirect.com/science/article/pii/0006291X77907215>.
- [10] R. J. Kurland, *Biochemical and Biophysical Research Communications* **88**, 927 (1979), ISSN 0006-291X, URL <http://www.sciencedirect.com/science/article/pii/0006291X79914979>.
- [11] M. Eisenberg, T. Gresalfi, T. Riccio, and S. McLaughlin, *Biochemistry* **18**, 5213 (1979).
- [12] H. Hauser and G. G. Shipley, *Biochemistry* **22**, 2171 (1983).
- [13] R. Dluhy, D. G. Cameron, H. H. Mantsch, and R. Mendelsohn, *Biochemistry* **22**, 6318 (1983).
- [14] H. Hauser and G. Shipley, *Biochimica et Biophysica Acta (BBA) - Biomembranes* **813**, 343 (1985), ISSN 0005-2736, URL <http://www.sciencedirect.com/science/article/pii/0005273685902512>.
- [15] G. W. Feigenson, *Biochemistry* **25**, 5819 (1986).
- [16] J. Mattai, H. Hauser, R. A. Demel, and G. G. Shipley, *Biochemistry* **28**, 2322 (1989).
- [17] M. Roux and M. Bloom, *Biochemistry* **29**, 7077 (1990).
- [18] M. Roux and M. Bloom, *Biophys. J.* **60**, 38 (1991).
- [19] J. M. Boettcher, R. L. Davis-Harrison, M. C. Clay, A. J. Nieuwkoop, Y. Z. Ohkubo, E. Tajkhorshid, J. H. Morrissey, and C. M. Rienstra, *Biochemistry* **50**, 2264 (2011).
- [20] J. Seelig, *Cell Biology International Reports* **14**, 353 (1990), ISSN 0309-1651, URL <http://www.sciencedirect.com/science/article/pii/030916519091204H>.
- [21] C. G. Sinn, M. Antonietti, and R. Dimova, *Colloids and Surfaces A: Physicochemical and Engineering Aspects* **282-283**, 410 (2006), a Collection of Papers in Honor of Professor Ivan B. Ivanov (Laboratory of Chemical Physics and Engineering, University of Sofia) Celebrating his Contributions to Colloid and Surface Science on the Occasion of his 70th Birthday.
- [22] R. M. Venable, Y. Luo, K. Gawrisch, B. Roux, and R. W. Pastor, *The Journal of Physical Chemistry B* **117**, 10183 (2013).
- [23] T. Piggot, *CHARMM36 POPS simulations (versions 1 and 2) 298 K 1.0 nm LJ switching* (2017), URL <https://doi.org/10.5281/zenodo.1129415>.
- [24] T. Piggot, *CHARMM36 POPS simulations (versions 1 and 2) 298 K 1.0 nm LJ switching with K ions* (2018), URL <https://doi.org/10.5281/zenodo.1182654>.
- [25] T. Piggot, *CHARMM36-UA POPS simulations (versions 1 and 2) 298 K 1.0 nm LJ switching* (2017), URL <https://doi.org/10.5281/zenodo.1129458>.
- [26] A. Maciejewski, M. Pasenkiewicz-Gierula, O. Cramariuc, I. Vattulainen, and T. Róg, *J. Phys. Chem. B* **118**, 4571 (2014).
- [27] T. Piggot, *MacRog POPS simulations (versions 1 and 2) 298 K with corrected PO not OP tails* (2018), URL <https://doi.org/10.5281/zenodo.1283335>.
- [28] M. Javanainen, *Simulation of a POPS membrane with potassium counterions* (2018), URL <https://doi.org/10.5281/zenodo.1434990>.
- [29] I. Gould, A. Skjerve, C. Dickson, B. Madej, and R. Walker, *Lipid17: A comprehensive amber force field for the simulation of zwitterionic and anionic lipids* (2018), in preparation.
- [30] I. S. Joung and T. E. Cheatham, *The Journal of Physical Chemistry B* **112**, 9020 (2008).
- [31] M. S. Miettinen and B. Kav, *Molecular dynamics simulation trajectory of an anionic lipid bilayer: 100 mol% POPS with Na+ counterions using Joung-Cheatham Ions* (2018), B.K. acknowledges financial support from International Max Planck Research School on Multiscale Bio-Systems., URL <https://doi.org/10.5281/zenodo.1148495>.
- [32] J. Åqvist, *J. Phys. Chem.* **94**, 8021 (1990).
- [33] M. S. Miettinen and B. Kav, *Molecular dynamics simulation trajectory of an anionic lipid bilayer: 100 mol% POPS with Na+ counterions using ff99 ions* (2018), B.K. acknowledges financial support from International Max Planck Research School on Multiscale Bio-Systems, URL <https://doi.org/10.5281/zenodo.1134869>.
- [34] P. Mukhopadhyay, L. Monticelli, and D. P. Tieleman, *Biophysical Journal* **86**, 1601 (2004).
- [35] T. Piggot, *Berger POPS simulations (versions 1 and 2) 298 K 1.0 nm cut-off* (2017), URL <https://doi.org/10.5281/zenodo.1129425>.
- [36] T. Piggot, *GROMOS-CKP POPS simulations (versions 1 and 2) 298 K with Berger/Chiu NH3 charges and PME* (2017), URL <https://doi.org/10.5281/zenodo.1129431>.
- [37] T. Piggot, *GROMOS-CKP POPS simulations (versions 1 and 2) 298 K with GROMOS NH3 charges and PME* (2017), URL <https://doi.org/10.5281/zenodo.1129435>.
- [38] J. P. M. Jämbek and A. P. Lyubartsev, *Phys. Chem. Chem. Phys.* **15**, 4677 (2013).
- [39] T. Piggot, *Slipids POPS simulations (versions 1 and 2) 298 K 1.0 nm cut-off with LJ-PME* (2017), URL <https://doi.org/10.5281/zenodo.1129441>.
- [40] T. Piggot, *CHARMM36 DOPS simulations (versions 1 and 2) 303 K 1.0 nm LJ switching* (2017), URL <https://doi.org/10.5281/zenodo.1129411>.
- [41] T. Piggot, *CHARMM36-UA DOPS simulations (versions 1 and 2) 303 K 1.0 nm LJ switching* (2017), URL <https://doi.org/10.5281/zenodo.1129456>.
- [42] B. Kav and M. S. Miettinen, *Molecular dynamics simulation trajectory of an anionic lipid bilayer: 100 mol% DOPS with Na+ counterions using Joung-Cheatham Ions* (2018), B.K. acknowledges financial support from International Max Planck Research School on Multiscale Bio-Systems, URL <https://doi.org/10.5281/zenodo.1134871>.
- [43] B. Kav and M. S. Miettinen, *Molecular dynamics simulation trajectory of an anionic lipid bilayer: 100 mol% DOPS with Na+ counterions using ff99 Ions* (2018), B.K. acknowledges financial support from International Max Planck Research School on Multiscale Bio-Systems, URL <https://doi.org/10.5281/zenodo.1135142>.
- [44] T. Piggot, *Berger DOPS simulations (versions 1 and 2) 303 K 1.0 nm cut-off* (2017), URL <https://doi.org/10.5281/zenodo.1129419>.

- [45] T. Piggot, *GROMOS-CKP DOPS simulations (versions 1 and 2) 303 K with Berger/Chiu NH3 charges and PME* (2017), URL <https://doi.org/10.5281/zenodo.1129429>.
- [46] T. Piggot, *GROMOS-CKP DOPS simulations (versions 1 and 2) 303 K with GROMOS NH3 charges and PME* (2017), URL <https://doi.org/10.5281/zenodo.1129447>.
- [47] T. Piggot, *Slipids DOPS simulations (versions 1 and 2) 303 K 1.0 nm cut-off with LJ-PME* (2017), URL <https://doi.org/10.5281/zenodo.1129439>.
- [48] F. Favela-Rosales, *MD simulation trajectory of a fully hydrated DOPS bilayer: SLIPIDS, Gromacs 5.0.4. 2017.* (2017), URL <https://doi.org/10.5281/zenodo.495510>.
- [49] J. J. López Cascales, J. García de la Torre, S. J. Marrink, and H. J. C. Berendsen, *The Journal of Chemical Physics* **104**, 2713 (1996).
- [50] S. A. Pandit and M. L. Berkowitz, *Biophysical Journal* **82**, 1818 (2002).
- [51] U. R. Pedersen, C. Leidy, P. Westh, and G. H. Peters, *Biochimica et Biophysica Acta (BBA) - Biomembranes* **1758**, 573 (2006).
- [52] P. T. Vernier, M. J. Ziegler, and R. Dimova, *Langmuir* **25**, 1020 (2009).
- [53] A. Martín-Molina, C. Rodríguez-Beas, and J. Faraudo, *Biophysical Journal* **102**, 2095 (2012).
- [54] P. Jurkiewicz, L. Cwiklik, A. Vojtšková, P. Jungwirth, and M. Hof, *Biochimica et Biophysica Acta (BBA) - Biomembranes* **1818**, 609 (2012).
- [55] J. Pan, X. Cheng, L. Monticelli, F. A. Heberle, N. Kucerka, D. P. Tieleman, and J. Katsaras, *Soft Matter* **10**, 3716 (2014).
- [56] S. Vangaveti and A. Travesset, *The Journal of Chemical Physics* **141**, 245102 (2014).
- [57] A. Melcrová, S. Pokorna, S. Pullanchery, M. Kohagen, P. Jurkiewicz, M. Hof, P. Jungwirth, P. S. Cremer, and L. Cwiklik, *Sci. Reports* **6**, 38035 (2016).
- [58] M. L. Valentine, A. E. Cardenas, R. Elber, and C. R. Baiz, *Biophysical Journal* **115**, 1541 (2018), ISSN 0006-3495, URL <http://www.sciencedirect.com/science/article/pii/S0006349518310221>.
- [59] M. J. Hallock, A. I. Greenwood, Y. Wang, J. H. Morrissey, E. Tajkhorshid, C. M. Rienstra, and T. V. Pogorelov, *Biochemistry* **57**, 6897 (2018).
- [60] S. Kim, D. Patel, S. Park, J. Slusky, J. Klauda, G. Widmalm, and W. Im, *Biophysical Journal* **111**, 1750 (2016), ISSN 0006-3495, URL <http://www.sciencedirect.com/science/article/pii/S0006349516307615>.
- [61] J. B. Klauda, R. M. Venable, J. A. Freites, J. W. O'Connor, D. J. Tobias, C. Mondragon-Ramirez, I. Vorobyov, A. D. MacKerell Jr, and R. W. Pastor, *J. Phys. Chem. B* **114**, 7830 (2010).
- [62] O. Berger, O. Edholm, and F. Jähnig, *Biophys. J.* **72**, 2002 (1997).
- [63] A. Botan, F. Favela-Rosales, P. F. J. Fuchs, M. Javanainen, M. Kanduč, W. Kulig, A. Lamberg, C. Loison, A. Lyubartsev, M. S. Miettinen, et al., *J. Phys. Chem. B* **119**, 15075 (2015).
- [64] A. Catte, M. Giry, M. Javanainen, C. Loison, J. Melcr, M. S. Miettinen, L. Monticelli, J. Maatta, V. S. Oganessian, O. H. S. Ollila, et al., *Phys. Chem. Chem. Phys.* **18**, 32560 (2016).
- [65] O. S. Ollila and G. Pabst, *Biochimica et Biophysica Acta (BBA) - Biomembranes* **1858**, 2512 (2016).
- [66] J. Melcr, H. Martinez-Seara, R. Nencini, J. Kolafa, P. Jungwirth, and O. H. S. Ollila, *The Journal of Physical Chemistry B* **122**, 4546 (2018).
- [67] H. U. Gally, G. Pluschke, P. Overath, and J. Seelig, *Biochemistry* **20**, 1826 (1981).
- [68] P. Scherer and J. Seelig, *EMBO J.* **6** (1987).
- [69] J. J. Madsen, *MD simulations of bilayers containing PC/PS mixtures and CaCl₂: 150POPC_150POPS_neutral* (2019), URL <https://doi.org/10.5281/zenodo.2542164>.
- [70] T. Piggot, *CHARMM36 POPS/POPC simulations (versions 1 and 2) 298 K 1.0 nm LJ switching with K ions* (2018), URL <https://doi.org/10.5281/zenodo.1182658>.
- [71] T. Piggot, *CHARMM36 POPS/POPC simulations (versions 1 and 2) 298 K 1.0 nm LJ switching with Na ions* (2018), URL <https://doi.org/10.5281/zenodo.1182665>.
- [72] J. J. Madsen, *MD simulations of bilayers containing PC/PS mixtures and CaCl₂: 250POPC_50POPS_0.15M CaCl₂* (2019), URL <https://doi.org/10.5281/zenodo.2542176>.
- [73] J. J. Madsen, *MD simulations of bilayers containing PC/PS mixtures and CaCl₂: 250POPC_50POPS_1M CaCl₂* (2019), URL <https://doi.org/10.5281/zenodo.2542135>.
- [74] J. J. Madsen, *MD simulations of bilayers containing PC/PS mixtures and CaCl₂: 250POPC_50POPS_neutral* (2019), URL <https://doi.org/10.5281/zenodo.2542151>.
- [75] M. Javanainen, *Simulation of a POPC bilayer at 298K, lipid model by Maciejewski and Rog* (2018), URL <https://doi.org/10.5281/zenodo.1167532>.
- [76] M. Javanainen, *Simulations of popc/pops membranes with cacl₂.* (2017), URL <https://doi.org/10.5281/zenodo.1409551>.
- [77] C. J. Dickson, B. D. Madej, A. A. Skjervik, R. M. Betz, K. Teigen, I. R. Gould, and R. C. Walker, *J. Chem. Theory Comput.* **10**, 865 (2014).
- [78] B. Kav and M. S. Miettinen, *Amber Lipid17 Simulations of POPC/POPS Membranes with KCl Counterions* (2018), B.K acknowledges financial support from International Max Planck Research School on Multiscale Bio-Systems, URL <https://doi.org/10.5281/zenodo.1250969>.
- [79] B. Kav and M. S. Miettinen, *Amber Lipid17 Simulations of POPC/POPS Membranes with NaCl Counterions* (2018), B.K acknowledges financial support from International Max Planck Research School on Multiscale Bio-Systems, URL <https://doi.org/10.5281/zenodo.1250975>.
- [80] B. Kav and M. S. Miettinen, *Amber Lipid17 Simulations of POPC/POPS Membranes with CaCl₂* (2018), B.K acknowledges financial support from International Max Planck Research School on Multiscale Bio-Systems, URL <https://doi.org/10.5281/zenodo.1438848>.
- [81] J. Melcr, *Molecular dynamics simulations of lipid bilayers containing POPC and POPS with the lipid17 force field, only counterions, and CaCl₂ concentrations* (2018), URL <https://doi.org/10.5281/zenodo.1487761>.
- [82] D. E. Smith and L. X. Dang, *J. Chem. Phys.* **100**, 3757 (1994), URL <http://scitation.aip.org/content/aip/journal/jcp/100/5/10.1063/1.466363>.
- [83] L. X. Dang, G. K. Schenter, V.-A. Glezakou, and J. L. Fulton, *J. Phys. Chem. B* **110**, 23644 (2006), ISSN 1520-6106, URL <http://dx.doi.org/10.1021/jp064661f>.
- [84] D. P. Tieleman, H. J. Berendsen, and M. S. Sansom, *Biophys. J.* **76**, 1757 (1999).
- [85] O. O. H. Samuli, *POPC:POPS (4:1) simulation with Berger model at 310K* (2018), URL <https://doi.org/10.5281/zenodo.1475285>.
- [86] C. Lukasz, *MD simulation trajectory of a POPC/POPS (4:1)*

- bilayer with 102mM CaCl₂, Berger force field for lipids, scaled charges for Ca²⁺ and Cl⁻ (2017), URL <https://doi.org/10.5281/zenodo.887398>.
- [87] C. Lukasz, MD simulation trajectory of a POPC/POPS (4:1) bilayer with 715mM CaCl₂, Berger force field for lipids, scaled charges for Ca²⁺ and Cl⁻ (2017), URL <https://doi.org/10.5281/zenodo.887400>.
- [88] T. Piggot, GROMOS-CKP POPS/POPC simulations (versions 1 and 2) 298 K with GROMOS NH3 charges and PME (2018), URL <https://doi.org/10.5281/zenodo.1283333>.
- [89] T. Piggot, GROMOS-CKP POPS/POPC simulations (versions 1 and 2) 298 K with Berger/Chiu NH3 charges and PME (2018), URL <https://doi.org/10.5281/zenodo.1283331>.
- [90] S. V. Dvinskikh, H. Zimmermann, A. Maliniak, and D. Sandstrom, J. Magn. Reson. **168**, 194 (2004).
- [91] J. D. Gross, D. E. Warschawski, and R. G. Griffin, J. Am. Chem. Soc. **119**, 796 (1997).
- [92] T. M. Ferreira, F. Coreta-Gomes, O. H. S. Ollila, M. J. Moreno, W. L. C. Vaz, and D. Topgaard, Phys. Chem. Chem. Phys. **15**, 1976 (2013).
- [93] T. M. Ferreira, R. Sood, R. Bärenwald, G. Carlström, D. Topgaard, K. Saalwächter, P. K. J. Kinnunen, and O. H. S. Ollila, Langmuir **32**, 6524 (2016).
- [94] M. Bak, J. T. Rasmussen, and N. C. Nielsen, Journal of Magnetic Resonance **147**, 296 (2000), ISSN 1090-7807, URL <http://www.sciencedirect.com/science/article/pii/S1090780700921797>.
- [95] N. Michaud-Agrawal, E. J. Denning, T. B. Woolf, and O. Beckstein, Journal of Computational Chemistry **32**, 2319 (2011), <https://onlinelibrary.wiley.com/doi/pdf/10.1002/jcc.21787>, URL <https://onlinelibrary.wiley.com/doi/abs/10.1002/jcc.21787>.
- [96] Richard J. Gowers, Max Linke, Jonathan Barnoud, Tyler J. E. Reddy, Manuel N. Melo, Sean L. Seyler, Jan Domański, David L. Dotson, Sébastien Buchoux, Ian M. Kenney, et al., in *Proceedings of the 15th Python in Science Conference*, edited by Sebastian Benthall and Scott Rostrup (2016), pp. 98 – 105.
- [97] ohsOllila and et al., *Match github repository*, URL <https://github.com/NMRLipids/MATCH>.
- [98] M. Abraham, D. van der Spoel, E. Lindahl, B. Hess, and the GROMACS development team, *GROMACS user manual version 5.0.7* (2015), URL www.gromacs.org.
- [99] H. Akutsu and J. Seelig, Biochemistry **20**, 7366 (1981).
- [100] C. Altenbach and J. Seelig, Biochemistry **23**, 3913 (1984).
- [101] J. Seelig, P. M. MacDonald, and P. G. Scherer, Biochemistry **26**, 7535 (1987).
- [102] F. Borle and J. Seelig, Chemistry and Physics of Lipids **36**, 263 (1985).
- [103] P. M. Macdonald and J. Seelig, Biochemistry **26**, 1231 (1987).
- [104] M. Roux and J.-M. Neumann, FEBS Letters **199**, 33 (1986).
- [105] P. G. Scherer and J. Seelig, Biochemistry **28**, 7720 (1989).
- [106] M. Roux, J.-M. Neumann, M. Bloom, and P. F. Devaux, European Biophysics Journal **16**, 267 (1988).
- [107] M. Loosley-Millman, R. Rand, and V. Parsegian, Biophysical Journal **40**, 221 (1982).
- [108] R. Rand and V. Parsegian, Biochimica et Biophysica Acta (BBA) - Reviews on Biomembranes **988**, 351 (1989).
- [109] J. Melcr, POPC lipid membrane, 303K, Charmm36 force field, simulation files and 200 ns trajectory for Gromacs MD simulation engine v5.1.2 (2016), URL <https://doi.org/10.5281/zenodo.153944>.
- [110] F. Favela-Rosales, MD simulation trajectory of a lipid bilayer: Pure POPC in water. SLIPIDS, Gromacs 4.6.3. 2016. (2016), URL <https://doi.org/10.5281/zenodo.166034>.
- [111] H. I. Petrache, S. Tristram-Nagle, K. Gawrisch, D. Harries, V. A. Parsegian, and J. F. Nagle, Biophysical Journal **86**, 1574 (2004).
- [112] S. Ollila, M. T. Hyvönen, and I. Vattulainen, J. Phys. Chem. B **111**, 3139 (2007).
- [113] G. Ceve, Biochim. Biophys. Acta - Rev. Biomemb. **1031**, 311 (1990).
- [114] Melcr and et al., *Eccpops github repository*, URL https://github.com/jmelcr/ecc_lipids.

ToDo

| | P. |
|---|----|
| 1. Authorlist is not yet complete | 1 |
| 8. Spell out REDOR? | 1 |
| 2. Correct citation for CHARMMua DOPS | 2 |
| 3. Correct citation(s) for CKP. | 2 |
| 4. Correct citation(s) for CKP. | 2 |
| 5. Correct citation for CHARMMua DOPS | 2 |
| 6. Correct citation(s) for CKP. | 2 |
| 7. Correct citation(s) for CKP. | 2 |
| 9. Should we leave the mention of ECC out from the Introduction (i.e., mention it only in the Conclusions) as the ECC parameters are not used in the paper? . . . | 2 |
| 10. citation needed? | 4 |
| 11. How long and how many repeats did this take approximately? Was the homogeneity determined visually? . . . | 4 |
| 12. There are ion number densities, right? | 4 |
| 13. I think that the peak labeling would be good to show also in (A). | 5 |
| 14. 2) Error bars? | 5 |
| 17. observed in the experiments? | 6 |
| 18. refer to experiments also? | 6 |
| 19. rather: narrow? | 6 |
| 20. detected, predicted, speculated? | 6 |
| 15. Figure clarity is questioned in: https://github.com/NMRLipids/NMRLipidsIVotherHGs/issues/48 . . . | 7 |
| 16. Commented by M. Javanainen in blog: MacRog pure POPS is simulated with Verlet cutoff scheme, Piggot is rerunning with group cutoff scheme. Check if affects results & update figures when ready | 8 |
| 22. can we really say this based on our data? We don't discuss hydrogen bonding | 8 |
| 21. After we know which force field is used for POPC in Gromos-CKP simulations, we might be able to add Gromos-CKP data into this plot. | 8 |
| 23. Why isn't this a problem with PC | 8 |
| 24. Should we include also counterions into the plot? . . . | 11 |